Coupled models for stress dissipation tests

E. Imre
Obuda University, EKIK HBM Systems Research Center, Banki Faculty, Budapest, Hungary,
imre.emoke@kvk.uni-obuda.hu

L. Bates L., S. Fityus
University of Newcastle, Newcastle, Australia

V. P. Singh
Texas A&M. University, USA

ABSTRACT: The dissipation tests are made by the staged oedometer tests and by the CPT or DMT and can be modelled by linear or non-linear coupled consolidation models. The coupled consolidation models of the staged oedometer tests, differing in one boundary condition (coupled 1: constant displacement, 2: constant total stress) are extended for larger space dimension *m* (oedometer:1, spherical:3, cylindrical:2) resulting in two model families. In this paper these models are analysed qualitatively and, numerically.
The pore water pressure data can be evaluated by the linear, coupled consolidation models. The displacement, total stress data can be evaluated by the non-linear coupled consolidation models. The solutions are surprisingly similar for the various *m* values, within a model family. At a fixed initial condition and dimension *m* the dissipation is faster for the coupled 1 than for the coupled 2 models. The time for dissipation - determined by the initial mean effective stress - decreases with *m*. The analytical solution is numerically simpler for *m*= 1 and 3 and more complicated for *m*=2 where it is approximated by a numerical series which is non-convergent for some space variable values. The total stress dissipation data can be evaluated with such linear models where the total stress is not constant rather decreases with time at the boundary. This condition is met for the coupled 1 models, where the total stress decrease during the dissipation test is related to the mean pore water pressure on the displacement domain. The non-linearity is approximated by a relaxation part-model (oedometric relaxation test, total stress dissipation test of CPT or DMT).

Keywords: keywords should use times new roman 10 pt. font; separated by semicolon; maximum 5

1. Introduction

1.1. The dissipation test evaluation

The dissipation type (staged) oedometer tests, cone penetrometer or flat dilatometer tests are used for the laboratory/in situ assessment of permeability/coefficient of consolidation by evaluating the measured data with a consolidation model (Tables 1 to 5, Fig. 1, [1 to 11]). The displacement and the total stress data are evaluated with non-linear consolidation model, taking into account the creep/relaxation, respectively, the pore water pressure data are evaluated with a linear model.

In the CPTu or DMT dissipation tests, not only the pore water pressure but also the radial total stress, (and the local side friction and cone resistance) can be recorded at the penetrometer – soil interface. The radial total stress, in soft clay may decrease by 73%, the effective stress may vary non-monotonically ([11]), decreasing or increasing during the first few minutes, depending on the soil plasticity and OCR.

Only the CPTu pore water pressure dissipation tests are evaluated at present in the practice. Approximate evaluation method is available for the DMT total stress dissipation test, assuming that the inflexion point of the measured curve is at 50 % consolidation. The reason for this is that constant total stress is assumed by the models available, no total stress dissipation is decribed.

1.2. The aim and content of the paper

Considering the uncoupled models and two point-symmetric consolidation model families, for every embedding space dimension *m*, there are three consolidation models which can be related three kinds of boundary conditions and can be used for the evaluation of some dissipation tests. These are the uncoupled and the two coupled models differing in one boundary condition at the outer, zero pore water pressure line boundary in the soil where the coupled 1 models apply displacement type boundary condition, the coupled 2 models apply constant total stress (constant volumetric strain).

According to [18], the pore water pressure solution of the coupled 2 models reduce to the one of the uncoupled models which apply the assumption that the total stress is constant.

The aim of the paper is (i) to proof the similarity of the linear, pointsymmetric, coupled mathematical models by expressing them as a special case of a single model with unique analytical solution such that all can be derived from this by inserting the proper boundary condition and embedding space dimension *m*, (ii) to characterize the analytical and numerical properties of the individual solutions (Table 3 to 5) in the function of the initial condition for fixed boundary conditions and space dimension, (iii) to suggest simple methods to take into account the non-linearity of the constitutive law.

In the first part of the paper the core model is given in the form of system of differential equations and analytical solution in terms of the dimension *m.* The structure of solution is treated. The analytical properties of the solution are analysed for the two kinds of boundary conditions, independently of the embedding space dimension *m*.

In the second part of the paper the constants of the solutions are presented in the function of the boundary conditions and the dimension *m*. Approximate closed form solutions for the boundary condition equations are given which are the same for the same boundary condition (within a model family). The solution is determined for each model. The convergence properties are characterized. The validation of the models is discussed.

The practical significance is that the analytical models can be used in the precise evaluation of the dissipation tests, eg., to reduce of the test duration and to evaluate the DMT total stress dissipation test data with no inflexion point, where no method is available.

Table 1 Types of one dimensional oedometric dissipation tests with constant boundary condition

(Multistage) relaxation test	(MRT)
(Multistage) compression test	(MCT)

Table 2 Types dissipation tests made with static penetrometers, modelled with cylindrical and spherical (ellipsoid) shaped domain.

Measured variable	dissipation test made by
Pore water pressure dissipation test, sensor on the shaft and/or on the tip	CPTu (static cone penetrometer)
Total stress dissipation test, sensor on the shaft and/or on the tip	CPTuσ, piezo-lateral stress cell DMTσ CPTq$_c$
Effective stress dissipation test, sensor on the shaft	CPTf$_s$

Table 3 1D point-symmetric consolidation models

V or ε boundary condition	1D (Oedometric models)
no (uncoupled)	Terzaghi (1923) [4]
v-*v* (coupled 1)	Imre (1997-1999) [5]
v-ε (coupled 2)	Biot (1941) [6]

Table 4 2D point-symmetric consolidation models

V or ε boundary condition	2D (Cylindrical pile models)
no (uncoupled)	Soderberg (1962) [7]
v-*v* (coupled 1)	Imre & Rózsa (1998) [2]
v-ε (coupled 2)	Randolph at al (1979) [1,8]

Table 5 3D consolidation models

v or ε boundary condition	3D (Spherical pile models)
no (uncoupled)	Torstensson (1975) [9]
v-*v* (coupled 1)	Imre & Rózsa (2002) [3]
v-ε (coupled 2)	Imre & Rózsa (2005) [10]

Note: uncoupled-like coupled model, the pore water pressure solution agrees with the uncoupled one ([19], Sills 1975).

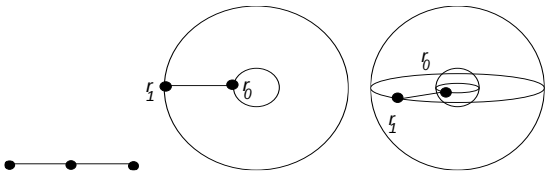

Figure 1. The displacement domain bounded by a (a) 0 dimensional sphere (oedometer model), (b) 1 dimensional sphere (cylindrical model), (c) 2 dimensional sphere (spherical model).

2. Point-symmetric consolidation models

2.1. System of differential equations

Two equations have been derived from the equilibrium condition and, from the continuity condition ([12]). Equation (1) compiles the equilibrium condition, the effective stress equality, the geometrical and, the constitutive equations, as follows:

$$E_{oed}\frac{\partial \varepsilon}{\partial r} - \frac{\partial u}{\partial r} = 0 \tag{1}$$

and, Equation (2) compiles the continuity equation, the Darcy's law (neglecting the gravitational component of the hydraulic head) and the geometrical equation, as follows:

$$-\frac{k}{\gamma_v}\Delta\, u + \frac{\partial \varepsilon}{\partial t} = 0 \tag{2}$$

where the volumetric strain and the Laplacian operator are as follows:

$$\varepsilon = \frac{1}{r^{m-1}}\frac{\partial}{\partial r}\left(r^{m-1} v\right) \tag{3}$$

$$\Delta = \frac{1}{r^{m-1}}\frac{\partial}{\partial r}\left(r^{m-1}\frac{\partial}{\partial r}\right) \tag{4}$$

v is the radial displacement, *u* is the excess pore water pressure, *r* and *t* are the space and the time co-ordinates respectively, E_{oed} is the oedometric modulus:

$$E_{oed} = \frac{2G(1-\mu)}{1-2\mu} = \frac{E(1-\mu)}{(1+\mu)(1-2\mu)}, \mu < 0.5 \tag{5}$$

G is the shear modulus, *E* is the is Young modulus, μ is the Poisson's ratio in terms of the effective normal stress σ' ($\sigma'=\sigma-u$ where σ is the total normal stress), *k* is the coefficient of permeability, γ_V is the unit weight of water.

2.2. Boundary conditions

Four boundary conditions are presented for *m*=2.

(1) The (common) *boundary condition Nr. 1* implies that the pore water pressure is zero at $r= r_1$:

$$u(t,r)|_{r=r_1} = 0 \tag{6}$$

(2) The (common) *boundary condition Nr. 2* entails that the flux is equal to zero at $r= r_0$:

$$\frac{\partial u(t,r)}{\partial r}|_{r=r_0} \equiv 0 \tag{7}$$

(3) The (common) *boundary condition Nr. 3* implies that the displacement equals to a constant at $r= r_0$:

$$v(t,r)|_{r=r_0} \equiv v_0 > 0 \tag{8}$$

(4) Boundary condition Nr. 4 – concerning the Imre-Rózsa model – implies that the displacement is zero at $r= r_1$:

$$v(t,r)|_{r=r_1} \equiv 0 \tag{9}$$

(5) *Boundary condition Nr. 5* - concerning the Randolph-Wroth model – expresses that the volumetric strain ε is constant $r= r_1$:

$$\varepsilon(t,r)|_{r=r_1} \equiv \varepsilon_1 > 0.$$

These boundary conditions are equally usable for m=3, in the case of m=1, $r_0 = 0$ is assumed, the half of the space domain is used.

2.3. Initial conditions

The initial condition for the pore water pressure is assumed to be given in the form of the following monotonic normalised parametric functions:

$$u_0(r,F) = \frac{1 - e^{\frac{r-r_1}{F}}}{1 - e^{-\frac{r_1-r_0}{F}}} \quad F \neq 0; \quad r_0 \le r \le r_1 \tag{11}$$

The value for u_0 at $r= r_0$ is equal to 1. The value for u_0 at $r= r_1$ is equal to 0. The mean:

$$D(F,r_0,r_1) = \frac{2}{r_1^2 - r_0^2} \int_{r_0}^{r_1} r u_0(r,F)\, dr \tag{12}$$

is used in the qualitative analysis and in the numerical examples. Analysing the shape function of the pore water pressure initial condition, it can be observed that parameters F and D are in one-to one relation. In the qualitative and quantitative analyse a shape function series is used with the mean initial pore water pressure values shown in Table 6.

Table 6. Initial condition parameter D [-]

u_0	1	3	4	7	8	9	10
D	0.001	0.053	0.135	0.408	0.591	740	0.970

3. Qualitative features of Solution

3.1. Structure of Solution

The structure of the solution can be determined on the basis of the concept of linear ordinary differential equations ([5]). The solution is equal to the following sum for each variable:

$$\bullet(t,r) = \bullet^p(r) + \bullet^L(r) + \bullet^t(t,r) + \bullet^w \tag{13}$$

where the superscripts p or L indicate the steady-state, drained continuum-mechanical or seepage problems resp., t indicates transient, w concerns the self-weight component.

The solution of the transient part satisfies the homogeneous form of the boundary conditions and its final value is zero. The solution of the steady-state part satisfies the inhomogeneous form of the boundary conditions.

3.2. Analysis of Equation (1)

By integrating the equilibrium Equation (1) with respect to r including boundary condition *Nr.* 1:

$$u(t,y) = E_{oed}\,\varepsilon(t,r) - E_{oed}\,\varepsilon(t,r)|_{r=r_1} \tag{14}$$

(10)

3.2.1. Coupled 1 model

A boundary condition function is derived by further integration between r_0 and r_1 using boundary condition *Nr.* 3 and boundary condition *Nr.* 4:

$$\varepsilon(t,r)|_{r=r_1} = -\left(\frac{u_{mean}(t)}{E_{oed}}\right) \tag{15}$$

where:

$$\varepsilon(t,r)|_{r=r_1} = -\left(\frac{u_{mean}(t)}{E_{oed}}\right) \tag{16}$$

$$u_{mean}(t) = \int_{r_0}^{r_1} u(t,r)\, dr \Big/ \int_{r_0}^{r_1} r\, dr \tag{17}$$

Inserting this boundary condition function into the equilibrium Equation:

$$u(t,r) = E_{oed}\,\varepsilon(t,r) + u_{mean}(t) \tag{18}$$

From this:

$$\varepsilon(t,r) = \frac{1}{E_{oed}}\left[u(t,r) - u_{mean}(t)\right] \tag{19}$$

It follows that for a realistic u the change in ε with t is positive in the vicinity at the outer boundary (rebound) and negative in the vicinity of the pile (compression). The final value of the transient strain is zero. By further integration:

$$v(t,r) = \frac{1}{rE_{oed}}\left(\int_{r1}^{r} ru(t,r)\, dr - u_{mean}(t) \int_{r1}^{r} r\, dr\right) \tag{20}$$

$$v(t,r) = \frac{1}{rE_{oed}}\left(\int_{r1}^{r} ru(t,r)\, dr - u_{mean}(t) \int_{r1}^{r} r\, dr\right) \tag{21}$$

It follows from the analysis of Equation (1) that for a realistic u the transient part of v is non-negative and, monotonously decreases with t for any r. The initial condition functions for u and v^t have the following relationships:

$$u_0(r) = E_{oed}\,\varepsilon_0^t(r) - E_{oed}\,\varepsilon_0^t(r)|_{r=r_1} \tag{22}$$

$$v_0^t(r) = \frac{1}{rE_{oed}}\left(\int_{r_1}^{r} ru_0(r)\, dr - u_{0,mean} \int_{r_1}^{r} r\, dr\right) \tag{23}$$

The Terzaghi's initial condition – where $u_0(r)$ is uniform with a positive value of c_1 – yields the following initial displacement function $v^t_0(r)$ for the coupled 1 model:

$$v_0^t(r) \equiv 0 \tag{24}$$

This is the zero solution function and the meaning is that the dissipation is instantaneous.

3.2.2. Coupled 2 model

Inserting the inhomogeneous form of boundary condition *Nr.* 5 into the equilibrium Equation:

$$u(t,y) = E_{oed}\,\varepsilon(t,r) \tag{25}$$

From this:

$$\varepsilon(t,y) = \frac{u(t,r)}{E_{oed}}. \tag{26}$$

It follows from the analysis of the equilibrium Equation that for a realistic u the change in ε with t is -negative (compression).By further integration:

$$v(t,r) = \frac{1}{rE_{oed}} \int_{r_0}^{r} ru(t,r)\,dr$$

It follows from the analysis of the equilibrium Equation that for a realistic u the transient part of v is non-negative and, monotonously decreases with t for any r. The initial condition functions for u, ε^t and v^t have the following relationships:

$$u_0(r) = E_{oed}\,\varepsilon_0^t(r) \tag{28}$$

$$v_0^t(r) = -\frac{1}{rE_{oed}} \int_{r_0}^{r} ru_0(r)\,dr. \tag{29}$$

The Terzaghi's initial condition – where the initial pore water pressure function $u_0(r)$ is uniform with a positive value of c_1 – yields the following initial displacement function $v^t_0(r)$ for the coupled 2 model:

$$v_0^t(r) = -\frac{c_1 r}{2E_{oed}}. \tag{30}$$

For a monotonic, positive initial pore water pressure function $u_0(r)$, compression and, as a result, in the vicinity of r_1 inward displacement takes place, the volume of the displacement domain is decreasing. The final value of the transient strain is zero.

3.3. Analysis of Equation (2)

The continuity Equation (2) can be written as follows by inserting the time dependent part of the volumetric strain ε^t:

$$-\frac{k}{\gamma_w}\Delta\, u + \frac{\partial \varepsilon^t}{\partial t} = 0 \tag{31}$$

By integrating the resulting equation twice with respect to r using the homogenous form of the boundary conditions *Nr.* 2 and *Nr.* 1 respectively, the following explicit expression can be derived for the pore water pressure:

$$u(t,r) = -\frac{\gamma_w}{k} \int_{r_1}^{t} \frac{1}{k} \int_{r_0}^{k} x \frac{\partial \varepsilon^t(t,x)}{\partial t}\,dx\,dk. \tag{32}$$

The pore water pressure function is further integrated with respect to t between 0 and ∞:

$$\int_0^{\infty} u(t,r)\,dt = -\frac{\gamma_w}{k} \int_{r_1}^{x} \frac{1}{k} \int_{r_0}^{k} [0 - x\varepsilon^t(0,x)]\,dx\,dk \tag{33}$$

It can be said that the initial value for the transient part of the volumetric strain (which can be written in terms of the initial pore water pressure) characterizes the rate of consolidation in every point. Especially, there is no time dependent consolidation if this function is the zero function.

3.4. Applications for the transient total and effective stress

The stress-state variable of the constitutive equation of the saturated soils is the effective stress, the difference of the total stress and the pore water pressure. The compression strain is positive. On the basis of u and ε the solutions, the total stress σ and the effective stress σ' can be assessed using the effective stress equality and the constitutive equations for embedding space dimension m=2:

$$\sigma = \sigma' + u. \tag{34}$$

$$\sigma_r' = -\frac{2G}{1-2\mu}\left[(1-\mu)\varepsilon - (1-2\mu)\frac{v}{r}\right] \tag{35}$$

$$\sigma_\varphi' = -\frac{2G}{1-2\mu}\left[\mu\varepsilon + (1-2\mu)\frac{v}{r}\right] \tag{36}$$

$$\sigma_z' = -\frac{2G\mu}{1-2\mu}\varepsilon \tag{37}$$

3.4.1. Coupled 1 model

The effective stresses at the shaft-soil interface:

$$\sigma_r'^t(t,r)|_{r=r_0} = -[u(t,r_0) - u_{mean}(t)] \tag{38}$$

$$\sigma_\varphi'^t(t,r)|_{r=r_0} = -\frac{\mu[u(t,r_0) - u_{mean}(t)]}{1-\mu} \tag{39}$$

It follows that for a realistic u the transient effective stress is negative around the shaft with zero final value and the effective stress at the shaft-soil interface increases with time here. It also follows that the effective stress at the outer boundary decreases with time, the mean of the first invariant of the effective stress tensor on the displacement domain is constant.

The radial total stress at the shaft-soil interface:

$$\sigma_r^t(t,r)|_{r=r_0} = u_{mean}(t) \tag{40}$$

It follows that for a realistic u the radial total stress at the shaft-soil interface decreases with time.

3.4.2. Coupled 2 model

The effective stresses at the shaft-soil interface:

$$\sigma_r'^t(t,r)|_{r=r_0} = -u(t,r) \tag{41}$$

$$\sigma_\varphi'^t(t,r)|_{r=r_0} = -\frac{\mu}{1-\mu}u(t,r) \tag{42}$$

It follows that for a realistic u the transient effective stress is negative around the shaft with zero final value and the effective stress at the shaft-soil interface increases with time. The radial total stress at the shaft-soil interface is constant with time.

$$\sigma_r^t(t,r)|_{r=r_0} = 0 \tag{43}$$

It follows that the radial total stress at the shaft-soil interface is constant.

3.5. Analytical Solution

3.5.1. Steady-state solution part

The solution of the drained continuum-mechanical problem for the displacement v^p is the solution of the following part of Equation (1):

$$E_{oed}\frac{\partial \varepsilon}{\partial r} = 0 \tag{44}$$

which is the cavity expansion model for m=2, 3 and the oedometer (K_0) compression model for m=1. The solution has the following general form:

$$v^p = \frac{\alpha}{r^{m-1}} + \beta r \tag{45}$$

where the parameters can be determined from the inhomogeneous form of the boundary conditions (i.e. the common boundary condition *Nr.* 3 and, `Nr. 4 - Imre-Rózsa model , Nr. 5 - Randolph-Wroth model)`.

These can be rewritten in the following form for m=2 as follows. The displacement v^p for the Imre-Rózsa model:

$$v^p(r) = \frac{r_0 v_0}{r_1^2 - r_0^2}\left(\frac{r_1^2}{r} - r\right). \tag{46}$$

and, for the Randolph-Wroth model:

$$v^p(r) = \frac{r_0 v_0}{r} + \frac{\varepsilon_1 r_0^2}{2r} + \frac{\varepsilon_1}{2} r. \tag{47}$$

The solution of the steady-state seepage problem for the pore water pressure u^L is identically equal to zero since the hydrodynamic boundary conditions are homogeneous. Therefore, superscript t is omitted for the pore water pressure in the following.

3.5.2. Transient solution part

The transient part of the displacement solution in the function of n (Imre et al, 2007):

$$v^t(t,r) = r^{\frac{-(m-2)}{2}} \sum_{k=1}^{\infty} C_k [J_{m/2}(\lambda_k r) + \mu_k Y_{m/2}(\lambda_k r)] e^{-[\lambda_k]^2 ct} \tag{48}$$

where $J_{m/2}$ and $Y_{m/2}$ are the Bessel functions of the first and second kinds, with the order of *m/2*, and λ_k, μ_k, C_k parameters of the solution, m is embedding space dimension. The volumetric strain and the pore water pressure solution from this:

$$\varepsilon^t(t,r) = r^{\frac{-(n-2)}{2}} \sum_{k=1}^{\infty} C_k \lambda_k \left\{[J_{(m-2)/2}(\lambda_k r) + \mu_k Y_{(m-2)/2}(\lambda_k r)]\right\} e^{-[\lambda_k]^2 ct} \tag{49}$$

The function u is then determined using Equation (1). For the Imre-Rózsa (i.e. m=2, coupled 1) model:

$$u(t,r) = \sum_{k=0}^{\infty} \lambda_k C_k e^{-\gamma_k^2 \cdot c_h \cdot t} \{[I_0(\lambda_k r) + \mu_k Y_0(\lambda_k r)] - [I_0(\lambda_k r_1) + \mu_k Y_0(\lambda_k r_1)]\} \tag{50}$$

and, for the Randolph-Wroth (i.e. m=2, coupled 2) model:

$$u(t,r) = \sum_{k=0}^{\infty} \gamma_k D_k e^{-\gamma_k^2 \cdot c_h \cdot t} [I_0(\gamma_k r) + \beta_k Y_0(\gamma_k r)]. \tag{51}$$

4. Numerical examples

Some numerical examples are given to illustrate the solution for m =2 and 3, the coupled 1 (Imre-Rózsa) models and coupled 2 (Randolph-Wroth) model for various inital conditions and space domains. Similar analyses were made for the oedometric case in ([5]). The results are mostly presented for m=2, on the example of r_0 =1.75 cm and r_1 = 64.75 cm, $n = r_1 / r_0$ = 37 (this space domain is about related to the undrained penetration problem of the CPT, well above the tip, see e.g. [20] (Baligh (1986)).

4.1. Definition of the numerical examples

The initial condition for the pore water pressure was given in the form of the following monotonic, normalised, parametric functions:

$$u_0(r,F) = \frac{1 - e^{\frac{r-r_1}{F}}}{1 - e^{-\frac{r_1-r_0}{F}}} \qquad F \neq 0; \quad r_0 \le r \le r_1 \tag{52}$$

The value for u_0 at r= r_0 is equal to 1 for every initial condition. The value for u_0 at r= r_1 is equal to 0 for every initial condition. The mean:

$$D(F, r_0, r_1) = \frac{2}{r_1^2 - r_0^2} \int_{r_0}^{r_1} r u_0(r,F)\, dr \tag{53}$$

was used to specify the numerical examples (Table 4). Analysing the shape functions of the pore water pressure initial condition (Fig. 2), it can be observed that parameters F and D are in one-to one relation. The shape functions are strictly convex, or concave, or linear. At the limits $F \to$-0 and, $F \to$+0, it is constant $u_0(r) \equiv 0$ and, $u_0(r) \equiv 1$, respectively, linear is the shape function at the limit where F equals to the plus or minus infinity (the D value is about equal to 0.33 and 0.5 in the cylindrical and oedometric case, resp.).

Ten values for the mean of the initial pore water pressure (parameter D) were selected, the value of parameter F was determined for each value of D and, for each value of r_1. The initial pore water pressure functions are shown in Figure 2(a) in the case of n=37 and in Figure 2(b) for other n values, where these were selected such that the D parameter was the same for the different r_1 values.

The initial displacement functions v^t_0 (r) were determined from $u_0(r)$ with the use of Eqs 21 and 27 (Part 1 paper) in each case (Fig. 3). The coefficients were determined from these using the orthogonality of the solution functions, in the case of m=2. The Bessel coefficients C_k and D_k from the initial displacement function v^t_0 (r):

$$C_k \text{ or } D_k = \frac{\int_{r_0}^{r_1} r\, v_0^t(,r)\left[J_1(\lambda_k r)+\mu_k Y_1(\lambda_k r)\right]dr}{\int_{r_0}^{r_1} r\left[J_1(\lambda_k r)+\mu_k Y_1(\lambda_k r)\right]^2 dr} \quad (54)$$

The boundary conditions were related to seven space domains with the same r_0 (Table 5). The precise roots of the boundary condition equations (λ_i, μ_i) were determined with the secant method for the case of the m =2 and 3 for the same of r_0 and seven values of $n= r_1 / r_0$, (Table 5). The number of terms was 40 at each specified r_0 and r_1, 250 terms were considered for n=37.

The following normalized space coordinate was applied representing the results on the space domain:

$$(r) = \frac{20(r - r_0) + (r_1 - r_0)}{r_1 - r_0} \quad (55)$$

4.2. Pore water pressure results

The rate of dissipation curve is controlled by the initial, transient mean effective stress. The dissipation is faster for the coupled 1 model than the coupled 2 model. For the coupled 2 model, as the distance from the zero solution is increasing (eg., in terms of the value of D), the dissipation time in terms of time factor (T_κ) increases for any κ (i.e. the curves "move" from left to right, see Fig 4(a)). For the coupled 1 model, having two zero solutions, the linear initial condition separates the dissipation curves solutions. If D<0.33 (i.e. convex initial distributions) or if D<0.33 (i.e. concave distributions) the dissipation time increases/decreases with increasing D. As a result, the dissipation curves related to some concave and convex initial condition functions coincide (Fig 4(b)).

The common features of the solution of the two models are as follows. According to the results shown in Figure 4 (a) and (b), for the not too extreme initial conditions (i.e. 4 to 7), the dissipation curve solutions are very similar. Especially, the dissipation curves coincide at great degrees of dissipation ($\kappa \approx 99{,}9\%$, $\kappa=(u_{max}-u)/u_{max}$). The time factor T_κ is about three times larger for the Randolph-Wroth's model, than for the Imre-Rózsa model resulting in larger dissipation times.

It can be observed that one-term solutions and the pore water pressure distribution after undrained penetration determined by the strain path method are roughly found in the strip of the four not too extreme initial conditions (i.e. 4 to 7, see Fig 2(b)). Therefore, the one-term solution, the solution related to the initial condition of the undrained penetration and, the solutions related to the initial conditions 4 to 7 are similar to each-other and can be interchanged.

Table 5. Displacement domains for the numerical tests (one value of r_0 and seven values of $n= r_1 / r_0$, r_0 =1.75 cm)

Serial number of domains	r_1 [cm]	$r_1 - r_0$ [cm]	$n=r_1/r_0$
1	7	5.25	4
2	33.25	31.5	19
3	64.75	63	37
4	127.75	126	73
5	255.5	253.75	146
6	511	509.25	292
7	1022	1020.25	584

4.3. Displacement, volumetric strain

The solutions for the transient displacement v^t and volumetric strain ε^t are shown in Figure 5. The transient part of the radial displacement v^t is non-negative and, basically decreases with t for any r up to zero in the case of both models. As a result, the inward displacement at the boundary r_1 is increasing in the case of the Randolph–Wroth model. The results for ε^t show compression in the case of the Randolph–Wroth model. Partly compression (in the vicinity of the shaft) and, partly swelling (at the outer boundary) takes place in the case of the Imre-Rózsa model.

4.4. Total stress results

Concerning the transient part of the solution for total stress, in the case of the Randolph-Wroth model (Fig. 6a) the radial total normal stress at r_0 is constant and, therefore, the radial effective stress at r_0 increases by the value of the initial pore water pressure at r_0. In the case of the Imre-Rózsa model the radial total normal stress at r_0 decreases with time by the value of initial pore water pressure D and, the radial effective stress at r_0 increases with time by the value of the difference of the initial mean pore water pressure and the initial pore water pressure at r_0 (Fig. 6b). The radial effective normal stress at the outer boundary decreases with time in the case of the Imre-Rózsa model and, is constant for the Randolph-Wroth model.

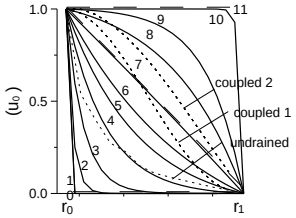

Figure 2. Initial pore water pressure, with the ones of the one-term solutions and the one determined by the strain path method, for n=37.

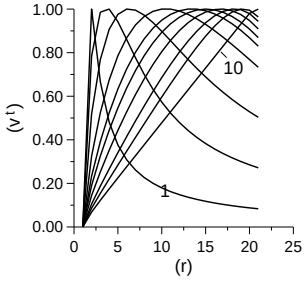

(a)

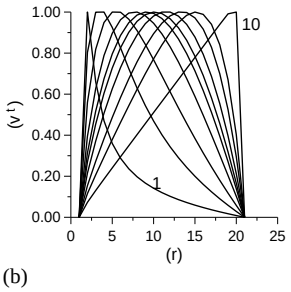

(b)

Figure 3. Initial conditions 1..10 concerning the transient part of the displacement for n=37 (a) Randolph-Wroth model, (b) Imre-Rózsa model.

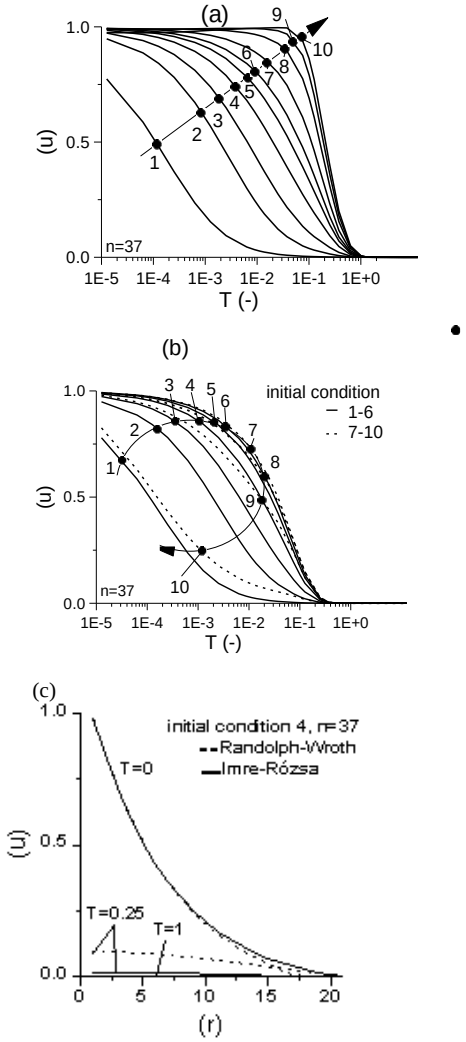

Figure 4. Pore water pressure solution. (a) to (c). Dissipation curves in the function of the initial condition for the Randolph-Wroth model, for the Imre-Rózsa model, comparing the results, resp. (d) Variation of the *u* with *t* and *r*.

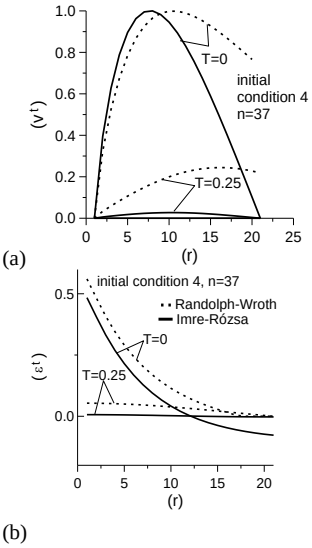

Figure 5. (a) Variation of the displacement v^t with t and r. (b) Variation of the volumetric strain ε^t with t and r

The sum of the solution of the drained continuum-mechanical problem and the self-weight was set to be equal to the initial value of the piezo-lateral stress cell measurement (see Figs 6, 7 [15]). A parametric analysis was made, the model constant displacement v_0 was computed for both models assuming μ=0.3, G=50 kPa and various values for K_0. Adding the transient and the so determined steady state parts, negative effective normal stresses were encountered within the displacement domain fr both models for small K_0 values (Figure 7). It follows that hydraulic fracturing may occur, in accordance to the experiences [24, 26-27].

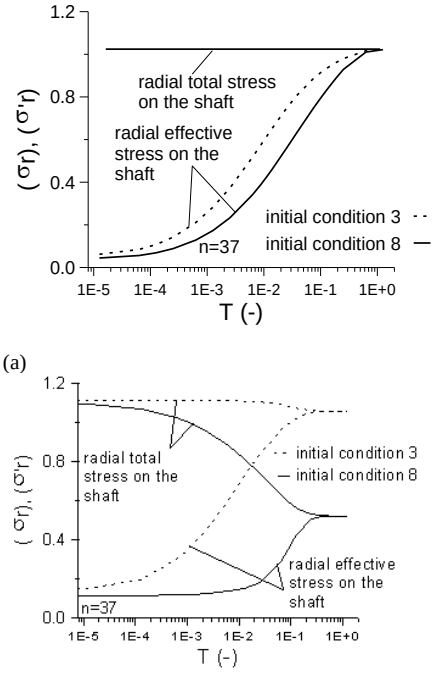

Figure 6. (a) and (b) The time variation of the transient component of the radial normal stresses acting on the shaft, cylindrical a. Randolph-Wroth model. b. Imre-Rózsa model, initial condition 8.

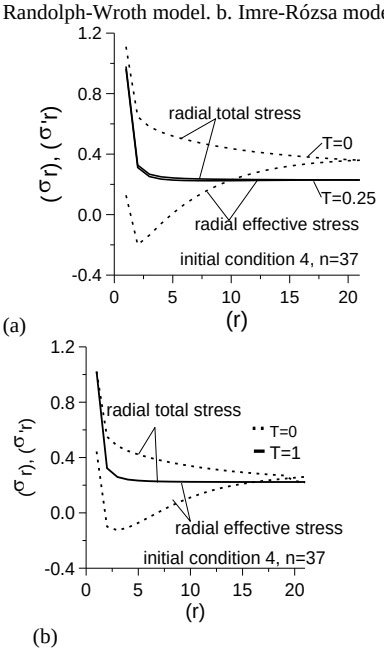

Figure 7. (a) and (b). Time variation of the radial normal stresses. Imre-Rózsa model and Randolph-Wroth model

5. Numerical tests on convergence

The numerical analyses were mostly related to space domain defined with radius r_0 =1.75 and r_1 = 64.75, embedding space dimension m=2 which is the case of undrained penetration, well above the tip.

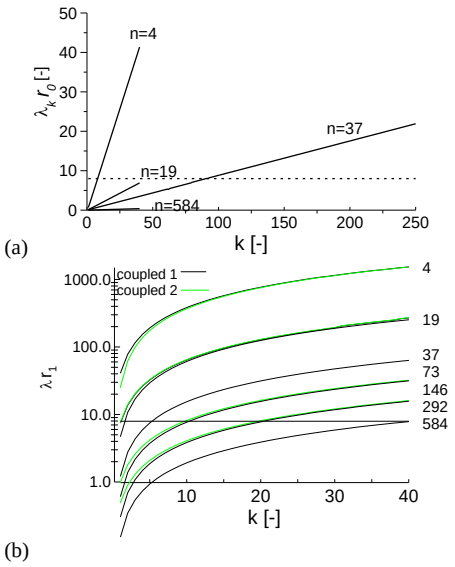

Figure 8. Bessel function approximation, cylindrical model (the preciseness of the analytical solution is acceptable below around 8 (a) and (b) Variation of the argument $r_0\lambda_k$ and $r_1\lambda_k$ with k and n (see Table 7).

5.1. Bessel function approximation, m=2

According the usual practice ([25, 30]), the Bessel function, of the first and second kinds, order of 1 and 0, which converge very slowly, were approximated by numerical series. These series were different in the small (x<8) and large (x>8) range of the independent variable. The small range functions look like simple power laws and were approximated by rational functions. The large range functions look like sine or cosine with decay of $x^{-1/2}$.

These numerical series – the products of polynomials and sine-cosine functions - were used in the form of a library routine ([30]). The series applied in the range x>8 was not convergent in the sense of convergence of power series, after a certain number the terms began to increase, even in the case of arbitrarily large x (semi-convergent series [25, 30]).

The separation of the two ranges can be seen in Figure 8 for the various space domains Table 7), noting that arguments are about the same for the two models on a given space domain. Concerning $x=r_0\lambda_k$ and $x=r_0\gamma_k$,, large is the range if k>8 for the smallest space domain (n=4) and if k>90 for the space domain of the dissipation test (n=37). Concerning $x= r_1\lambda_k$ and $r_1\gamma_k$, they were in the large range if k>3 for the space domain of the dissipation test (n=37), and for every k in case of the smallest domain, n=4 (see Table 7).

It follows that for n=37 the shaft stresses can be computed by the small range approximation precisely, however, at r_1 k~3 terms can be used in the small range approximation only. In the case for small displacement domains (e.g. n=4) at r_0 k~8 terms can be used in the small range approximation, at r_1 the large range approximation has to be used which may entail some convergence problems. The few terms in the small range approximation may entail non-precise solution.

Concerning the Imre-Rózsa model, the small range approximation series after summation was convergent with k up to about 200 terms then it became divergent for initial conditions 1 and 10. Concerning the Randolph-Wroth model, in the small range approximation after around 125 terms the series became divergent for most initial conditions.

5.2. The convergence in terms of initial condition shape function

The rate of convergence of the Fourier-Bessel expansion of the pore water pressure at $r=r_0$ was tested in the function of the initial condition shape functions (Table 6) for seven space domains (Table 7) and model. The value of 1 was approximated as follows:

$$1 = u_0(r_1, D, r_0) = \sum_{i=0}^{\infty} C_i \begin{Bmatrix} [I_0(\lambda_i r_0) + \mu_k Y_0(\lambda_i r_0)] \\ -[I_0(\lambda_i r_1) + \mu_k Y_0(\lambda_i r_1)] \end{Bmatrix} \quad (56)$$

$$1 = u_0(r_1, D, r_0) = \sum_{i=0}^{\infty} E_i [I_0(\gamma_i r_0) + \beta_i Y_0(\gamma_i r_0)] \quad (57)$$

The first k terms were considered. The results are summarized in the function of the initial conditions, space domain and number of terms in Figure 9, for the case of k<41, n=37. The error related to a certain k is rapidly increasing as the mean initial condition ordinate D varies 'towards' the D value of the closest zero solution (i.e. $D\rightarrow 0$ for both models, $D\rightarrow 1$ for the Imre - Rózsa model). For the not too extreme initial conditions (i.e. 3 to 7), the numerical error is not important.

This convergence property can be explained as follows. Since as the initial condition series "converges" to the zero solution, the coefficients converge to zero, and - being any other term constant in Equations (56)-(57) -, the sum will decrease at every fixed k if the initial condition 'is closer' to the zero solution. The decrease of the coefficients in terms of the initial conditions serial number can be seen in Figure 10.

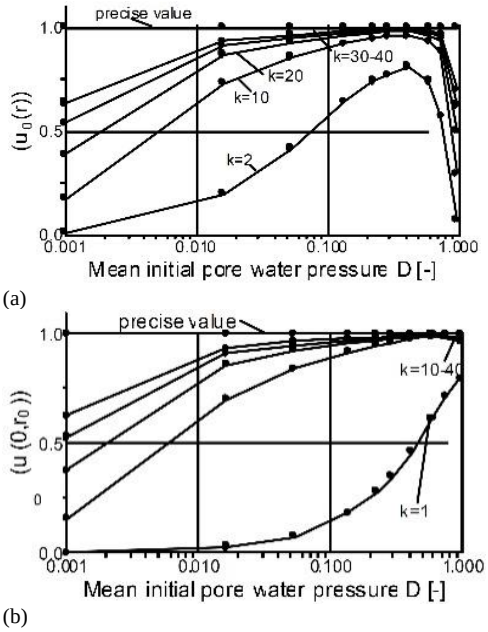

Figure 9. (a), (b). The Bessel series approximation of the initial u at r=r0 on the shaft (i.e. the precise is 1), in the function of D and k, n=37). The initial condition with serial number 1, 2 …10 is with D=0.001,0.016, ...0.970, resp, according to Table 6.

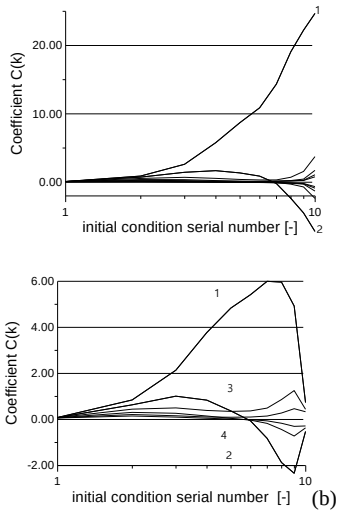

Figure 10. The coefficients for fixed k, depending on the serial number of the shape function. a. Randolph-Wroth model. b. Imre-Rózsa model. Note: The zero solution is related to the constant initial conditions with D =0 and 1 for the coupled 1 model, with D =0 for the coupled 2 model. The initial condition with serial number 1, 2 …10 with D=0.001,0.016, ...0.970, is in Table 6.

6. Approximate root formulae

6.1. Boundary conditions, root formulae

For the coupled 1 or 2 model-families, the "boundary condition equation" (arisen from the homogeneous form of boundary conditions Nr.3 and Nr.4 or Nr.3 and Nr.5) can be written as follows, respectively:

$$J_{m/2}(\lambda_k r_0)Y_{m/2}(\lambda_k r_1)-J_{m/2}(\lambda_k r_1)Y_{m/2}(\lambda_k r_0)=0 \quad (58)$$

$$J_{m/2}(\lambda_k r_0)Y_{(m-2)/2}(\lambda_k r_1)-J_{(m-2)/2}(\lambda_k r_1)Y_{m/2}(\lambda_k r_0)=0 \quad (59)$$

The roots of the boundary condition equation for the coupled 1 and 2 model-families, respectively, for m=1:

$$\lambda_k = \frac{k\pi}{(r_1-r_0)}, \quad \gamma_k = \frac{(2k-1)\pi}{2(r_1-r_0)} \quad (60)$$

Approximate closed form solution can be suggested as follows for m>1. The asymptotical Bessel function formulae:

$$\mathrm{J_n(r)} = \sqrt{\frac{2}{\pi r}}\cos\left(\mathrm{r}-\frac{\pi}{4}-\frac{\mathrm{n}\pi}{2}\right) \quad (61)$$

$$\mathrm{Y_n(r)} = \sqrt{\frac{2}{\pi r}}\sin\left(\mathrm{r}-\frac{\pi}{4}-\frac{\mathrm{n}\pi}{2}\right) \quad (62)$$

Using the asymptotical Bessel function formulae, the approximate form for the BCE for the coupled 1 and 2 model-families, respectively:

$$\sin(\lambda_k(r_1-r_0))=0 \quad (63)$$

$$\sin(\gamma_k(r_1-r_0)+\pi/2)=0. \quad (64)$$

being equally valid for dimensions embedding space dimension m=2 or 3. The roots for the coupled 1 and 2 model-families, respectively:

$$\lambda_k \approx \frac{k\pi}{(r_1-r_0)}, \gamma_k \approx \frac{(2k-1)\pi}{2(r_1-r_0)} \quad (65)$$

Within model-family 1, the 1 dimensional and the approximate 2 and 3 dimensional formulae are identical. Inserting into the analytic solutions, the following dimensionless variables are resulted:

$$(r)=\frac{r}{r_1-r_0} \quad (66)$$

$$T=\frac{ct}{(r_1-r_0)^2}. \quad (67)$$

These ensure that the solutions related to different space domains can approximately be transformed into each other. Slightly different formulae can be derived for the coupled 2 model family, reflecting that the rate of dissipation is faster for the coupled 1 than for the coupled 2 models.

$$(r)=\frac{r}{r_1-r_0} \quad (68)$$

$$T=\frac{ct}{(r_1-r_0)^2}. \quad (69)$$

6.2. Validity of the root formulae

In the case of the two cylindrical models (m =2), 250 terms were considered for n=37 and 40 for other space domains. The precise roots of the boundary condition equations were determined with the secant method and, were transformed using the approximate closed form formulae. The results are shown in Figure 11. According to the results, the error of the approximate closed form formulae decreases with k for both models. The validity of the approximate model law can numerically be proven for one-term solution and for "non-extreme" initial conditions ([31, 32]).

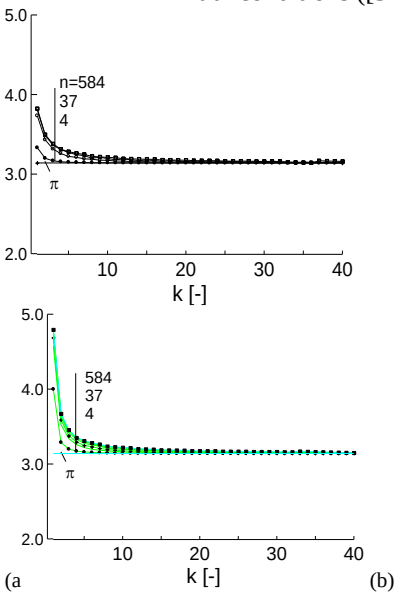

Figure 11. The validity of the approximate root formulae. . (a) (b) Results of the numerical tests for $\Pi=(r_1-r_0)\ \lambda_k/k$ *or* $\Pi=2(r_1-r_0)\ \gamma_k/(2k-1)$ using various values for r_1=n r_0 and r_0=1.75 cm.

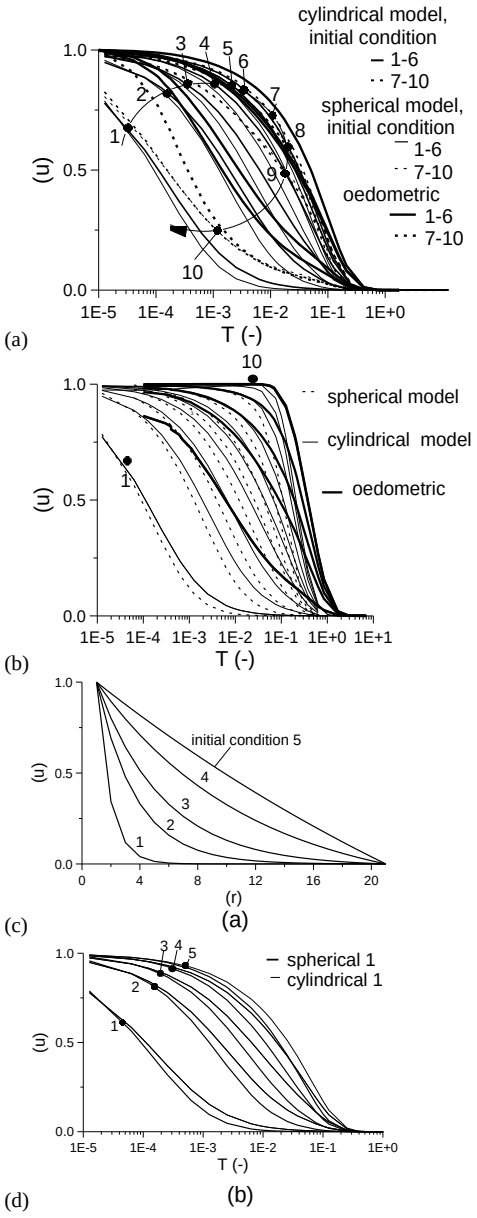

Figure 12. Similarity on the spherical, cylindrical and oedometric models dissipation curves, the tiny difference is related to the geometry of the displacement domain.

7. Dissipation test evaluation

7.1. The time factors

In this work approximate closed form solutions were given for the boundary condition equation in the two and three dimensional cases. It was found that, within a model-family, the precise (1 dimensional case) and the approximate (2 and 3 dimensional cases) roots of the boundary condition equation are identical.

This result allows the introduction of a new time factor in the transient solution part, differing by a constant multiplier from the one usually applied with space constant r0. The appearance of the time factor T ensures that the solutions related to different space domains can (approximately) be transformed into each other. The new time factor:

$$T = \frac{ct}{(r_1 - r_0)^2} = \frac{ct}{r_0^2\left(\frac{r_1}{r_0} - 1\right)^2} \quad \text{or}$$

$$T = \frac{ct}{4(r_1 - r_0)^2} = \frac{ct}{4r_0^2\left(\frac{r_1}{r_0} - 1\right)^2} \qquad (70)$$

It was shown that within a model-family, the precise (1 dimensional case) and the approximate (2 and 3 dimensional cases) roots of the boundary condition equation are identical.

7.2. The pore water pressure dissipation

Two kinds of staged oedometer tests are known with either total stress load or with displacement load. The related coupled consolidation models differ in one boundary condition, constant displacement at the trivial boundary and constant total stress or displacement is assumed at the non-trivial, loaded boundary, resp. According to experiences for the staged oedometer tests, non-linear constitutive law is needed for the displacement or total stress dissipation data (which can approximately be modeled by adding a creep and a relaxation part-model to the consolidation part-model).

In case of the coupled modelling of the dissipation tests, unmoved boundary is assumed at the penetrometer surface hiv. The two model-families can be defined by defining the boundary condition either at the zero pore water pressure line as constant total stress or as constant diaplacement. These are illustrated by some similar cases, the single drained oedometric test models (compression test and relaxation test). A boundary is unmoved in both cases, with zero u. The total stress is kept constant and creep can be observed during the compression test. The displacement load is kept constant, the total stress relaxation can be observed in the relaxation test. In the total stress or displacement modelling of the oedometer tests, the time dependent constitutive law is considered (creep and relaxation, resp. for the coupled 1 and 2 models, [27-28]).

The Randolph-Wroth model available for CPTu total stress dissipation gives no total stress dissipation at the penetrometer surface since it results in constant total stress at the shaft, similarly to the oedometric compression test model.

In this research displacement type boundary condition was assumed at the outer, unknown boundary (ie., at the zero pore water pressure line, [20]) generating a second model family, called coupled 1 models, being related to a rare type of the oedometer tests, the oedometer relaxation test.

The coupled 1 model assumes unmoved boundary, the coupled 2 model assumes constant total stress boundary at the zero pore water pressure line, in the soil mass. It is shown here, that the coupled 1 model results in total stress dissipation at the shaft surface.

At present both cylindrical models are used for the evaluation of the CPTu *u* tests in the frame of mathematically precise inverse problem solution ([11] to [14]). In addition, a numerical solution of an

uncoupled two-dimensional models is applied presently for approximate model fitting based on the use of the rigidity index 15 ([22] Baligh & Levadoux, 1986, [14] Teh & Houlsby, 1988).

This practice is in agreement with the fact that the analytical and numerical pore water pressure dissipation solution agree, as shown in Figure 15 (related to Ir=150 and the conventional time factors).Concerning the two model families, the dissipation curve solutions nearly agree, the (newly introduced) time factor values are increasing slightly with decreasing embedding space dimension due to geometrical reasons (Fig. 12). The point-symmetric and the true 2-dimensional solutions agree, also, the difference is tiny for some typical initial conditions (Fig. 13).

The analytical solutions for u can be easier computed in the case m=1 or 3 using sin and cosine functions. For m=2, Bessel functions are needed which are approximated due to the slow convergence and, the so resulted series is 'semi-convergent', becomes divergent after a while. The simplest numerical work is related to the oedometric models where no numerical solution is needed for the roots.

The analytical solutions are very useful in case of non-monotonic initial conditions, the dissipation curve is non-monotonic (Fig. 14) which may occur in CPTu testing if the soil is OC around the shaft (can originally be OC clay or can be a highly compressed sand or silt due to penetration which rebounds around the shaft) [31-32]. The modelling of non-monotonic dissipation curve is easier with the analytical models.

7.3. The total stress dissipation

The total stress solutions of the coupled 1 models with various embedding space dimensions *m*=1 to 3 are qualitatively similar. However, the controlling parameter (the mean initial normalized pore water pressure *D*) is significantly different for various the embedding space dimensions (i.e. for the linear function: D~1/(*m*+1)).

According to the first model validation results using oedometric relaxation test data, the time dependency of the constitutive law is needed to be considered. In the present form a relaxation term is added ([28] to [30]) as follows:

$$\sigma_r\ (t, r_0) = \sigma_r^c\ (t, r_0) + \Delta\sigma_r^r\ (t, r_0) \tag{71}$$

where superscripts *c* and *r* indicate consolidation and relaxation, respectively. The relaxation term:

$$\Delta\sigma_r^r\ (t, r_0) = -s \cdot \sigma(0, r_0) \cdot \log\frac{t}{t_1}; t > t_1 \tag{72}$$

where *s* is the coefficient of relaxation (typical values are between 0.02 to 0.08 for space dimension one), and t_1 is the delay time. The relaxation term is zero if $t \le t_1$. (Similar model is used for the stepwise compression test by adding a creep term, see App.1.).

The measurement made with the piezo-lateral stress cell in Boston Blue Clay ([15], Baligh et al (1985)) showed that the radial total stress at the shaft decreased by 73% of its value valid immediately after penetration. The effective stress decreased in the first minutes, then increased up to the end of the measurement when its value was about equal to the horizontal effective stress 'at rest' valid prior penetration. For longer time span, it may decrease again due to the relaxation ([23]).

Concerning the evaluation of the result of the piezo-lateral stress cell total stress dissipation test, it was found that the solution of the 2-dimensional, coupled 1 model with a realistic shape function and with a relaxation term may give too small total stress drop. The explanation is that the equipment lateral diameter may slightly change due to the stress release being not rigid [11]. Therefore, an extra total stress drop term was suggested for the routine evaluation of the DMT total stress dissipation tests [17]. This can be realized by selecting an initial condition shape function with 'large' mean coordinate *D*.

It can be noted that the evaluation of the relaxation test showed that the effective stress variation may be dependent on soil permeability and plasticity (see App.1). The consolidation increase may be suppressed by the relaxation decrease in clays and may not be suppressed by the relaxation decrease in sand in the first minutes of the test. In longer times opposite tendencies may occur.

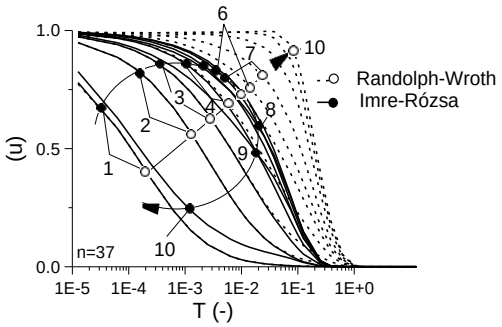

Figure 13. Dissipation curves in the function of the initial condition for the Randolph-Wroth model, for the Imre-Rózsa model, comparing the results.

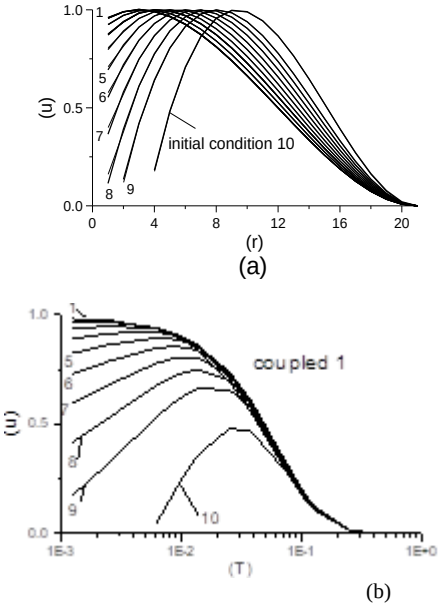

Figure 14. Comparing spherical dissipation curves, non-monotonic initial conditions for CPTu evaluation.

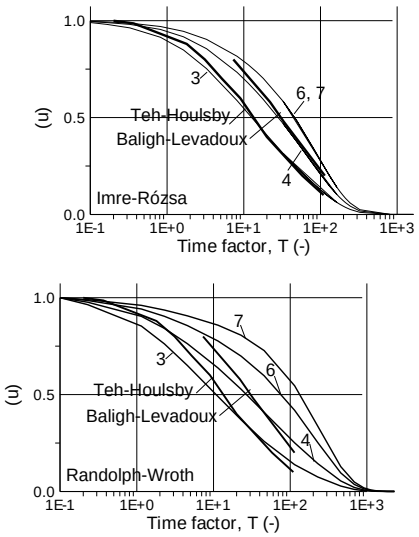

Figure 15. Comparing the Imre-Rózsa model with two dimensional solutions (initial conditions 3 to 6). (b) Comparing the Randolph-Wroth model with two dimensional solutions (initial conditions 3 to 7).

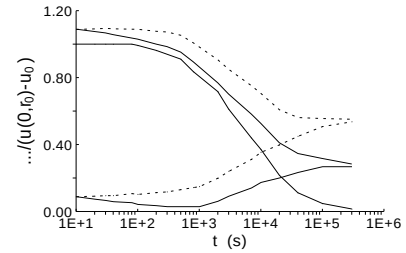

(a)

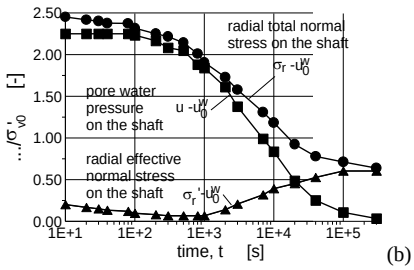

(b)

Figure 16. (a) Time variation of the radial normal stresses acting on the shaft, cylindrical joined 1 model, with unrealistic initial condition 8 (consolidation: dashed line, with the addition of a relaxation term: solid line). (b) Piezo-lateral stress cell measurement in clay (after [15], (Baligh et et al, 1985)).

8. Conclusions

(1) Considering the linear, point-symmetrics coupled consolidation models, for every space dimension *m*, two models were presented here. They differ in the boundary condition at the outer, unknown boundary within the soil at the zero pore water pressure line. The coupled 1 model assumes here constant displacement, the coupled 2 model assumes constant volumetric strain (and mean effective stress) here.

(2) Concerning the total stress dissipation, considerable total stress drop is encountered during the tests and the effective stress variation is non-monotonic. Only the coupled 1 models can be acceptable for the evaluation of the total stress dissipation tests since coupled 2 models prognosticate constant total stress at the shaft.

Furthermore, in the modelling of the CPT or DMT total stress dissipation tests, the coupled 1 models can be applied if the relaxation is also modeled, a relaxation model is superimposed to a coupled 1 model. The non-monotonic effective radial stress variation cannot qualitatively be described without relaxation.

In addition, a correction function is needed on the basis of the first evaluation results since the penetrometer surface is laterally not unmoved due to the stress release.

In conclusion, in the modelling of the CPT or DMT total stress dissipation tests, relaxation model is superimposed to a coupled 1 model and a correction function is needed.

(3) Being the analytical solutions similar for the coupled 1 model family, it may occur that – using the approximate time factor concept derived here - the models and the tests are interchanged. For example, the oedometric tests can be used to study the phenomena after pile penetration. Moreover, the dissipation test data measured after pile penetration can be evaluated with an oedometric model (ie., in other words, coupled 1 models for m= 1 and m=2 can be interchanged).

(4) The numerical simulations concerning undrained penetration, using the strain path solution of Baligh and the piezo-lateral stress cell data indicated that the effective stress may be negative in the vicinity of the shaft-soil interface after pile penetration (in the function of the K0 or at rest condition) since the transient part of the analytical solution is negative.

(5) Further theoretical and experimental research is suggested on this and on in many aspects, for example on the effects of time dependent constitutive law and boundary condition (slightly moving boundary in case of non- perfectly rigid pile material). Very few pieces of information are available on the initial condition of partly drained penetration and the emprirical relaxation law around piles.

References

[1] Burns, S.E., Mayne, P.W. Coefficient of consolidation ch from type 2 piezocone dissipation test in overconsolidated clay. Proc. of Int.Symp. on CPT. 1995. 137-142.

[2] Imre, E. and Rózsa, P. Consolidation around piles. Proc. of 3rd Sem. on Deep Found. on Bored and Auger Piles. Ghent 1998. 385-391.

[3] Imre, E. and Rózsa, P. Modelling for consolidation around the pile tip. Proc. of the 9th Int. Conf. on Piling and Deep Foundations DFI, Nizza. 2002. 513-519

[4] Terzaghi, K. Theoretical Soil Mechanics. Wiley: New York, 1948. 1-510.

[5] Imre, E. Consolidation models for the incremental oedometric tests. Acta Technica Acad. Sci. Hung. 1997-1999. 369-398.

[6] Biot, M. A. Theory of elasticity and consolidation for porous anisotropic solid. Jl. of Appl. Phys. 1955. 26:182-185.

[7] Soderberg, L. O.. Consolidation Theory Applied to Foundation Pile Time Effects. Geotechnique, 1962.12. 217-232.

[8] Randolph, M. F. & Wroth, C. P.. An analytical solution for the consolidation around displacement piles. I. J. for Num. Anal. Meth. in Geomechanics, 1979 3:217-229.

[9] Torstensson, B. A. The pore pressure probe. 1977. Paper No. 34. NGI

[10] Imre, E. and Rózsa, P. Modelling for consolidation around the pile tip. Proc. of the 9th Int. Conf. on Piling and Deep Foundations DFI, Nizza. 2002. 513-519

[11] Imre E, Rózsa P, Bates L, Fityus S. Evaluation of monotonic and non-monotonic dissipation test results. COMPUTERS AND

GEOTECHNICS 2010 37: 7-8. 885-904. DOI: 10.1016/j.compgeo.2010.07.008
[12] Imre, E.: Evaluation of "short" dissipation tests. Proc. of the 12th Danube-European Conference. 2002. 499-503.
[13] Lunne, T; Robertson, P.K.; Powell, J.J.M.. Cone Penetration testing. Blackie Academic & Professional; 1992. 1-312.
[14] Teh, C.I. and Houlsby, G.T.. Analysis of the cone penetration test by the strain path method. Proc. 6th Int. Conf. on Num. Meth. in Geomechanics, Innsbruck. 1988.
[15] Baligh, M. M.; Martin, R. T.; Azzouz, A. S.& Morrisson, M. J. The piezo-lateral stress cell. Proc. of the 11th ICSMFE San Francisco. 1985. 2:841-844.
[16] Totani, G; Clabrese, M; and Monaco, P. In situ determination of ch by flat plate dilatometer. Proceedings of ISC-1, Atlanta, Georgia, 1998. 883–888.
[17] Imre E, Bates L, Fityus S 2011 Evaluation of dilatometer dissipation test data with no inflexion point. In: Proc 13th International Conference of the International Association for Computer Methods and Advances in Geomechanics: IACMAG 2011. Melbourne. 2011.05.09-2011.05.11. pp. 495-501.
[18] Imre, E. Statistical evaluation of simple rheological CPT data. Proc. of XI. ECSMFE, Copenhagen, (1995). Vol. 1. 155-161.
[19] Sills, G. C Some conditions under which Biot's Equations of Consolidation Reduce to the Terzaghi's equation. Geotechnique, 1975. 251: 129-132.
[20] Baligh, M. M. Undrained deep penetration, II. pore pressures. Geotechnique, 1986. 364: 487-503.GGGG
[21] Lehane, B. M.; Jardine, R. J. Displacement-pile behaviour in a soft marine clay Canadian Geotechnical Journal. 1994. 31. 181-191.
[22] Baligh, M. M.; Levadoux, J. N. Consolidation after undrained penetration. II. Interpretation. Jl. of Geot. Eng. ASCE, 1986. 1127: 727-747.
[23] Yang, N.-C. Redriving characteristics of piles. ASCE Jl. of Soil Mech. and Found. Div. 1956.
[24] Massarch, K. R., Broms, B. B. 1977. Fracturing of Soil Caused by Pile Driving in Clay. Proc. of the 9th ICSMFE Tokyo, Vol.1. 197-200.
[25] Kármán, T. & Biot, M. A. Mathematical Meth. in Eng. McGraw-Hill. (1940).
[26] Peuchen J., Meijninger B. DrummenT 2015. Reassessment of geotechnical conditions after an offshore well incident. Proceedings of the XVI ECSMGE Geotechnical Engineering for Infrastructure and Development
[27] Imre E., Schanz T. and Vijay P. Singh (2013) Evaluation of staged oedometric tests 251-268. Proc. of the 3rd Kézdi Conference. Budapest, Hungary, 2013.05.28.ISBN 978-963-313-081-0
[28] Imre E., Schanz T., Hortobágyi Zs., Singh V.P., Fityus S. (2015) Oedometer relaxation test Proc. XVIECSMGE
[29] Imre E., Trang P.Q., Fityus S., Telekes G. A (2011) "Geomeric parameter error estimation method for inverse prolems." Proceedings of the Second International Symposium on Computational Geomechanics (ComGeo II), Cavtat, Croatia, 27-29 April, 2011.
[30] Press, W.H.; Flannery, B.P.; Teukolsky, S.A.; Wetterling, W.T. (1986): Numerical Recipes. Cambridge Univ. Press, Cambridge
[31] Imre, E, Rózsa, P (2010) some features of the coupled consolidation models used for the evaluation of the dissipation test. 7th European Conference on Numerical Methods in Geotechnical Engineering June 2 - 4, 2010Trondheim, Norway. p. 303-310
[32] E., Imre ; T., Schanz ; L., Bates ; S., Fityus. Evaluation of complex and/or short CPTu dissipation tests In: Michael, Hicks; Federico, Pisanò; Joek, Peuchen (szerk.) Cone Penetration Testing 2018 : Proceedings of the 4th. International Symposium on Cone Penetration Testing. London, Egyesült Királyság / Anglia : CRC Press (2018) 756 p. pp. 351-357.

1. APPENDIX

1.1. Some notes on the evaluation of u_2 tests – summary of newer methods

The two, suggested evaluation methods (slow, fast) differ in computer work, which is smaller by about 2 order of magnitudes for the fast method.

In the fast method, the output includes the C_i (I = 1 to k) linearly dependent coefficients for a few terms, the c nonlinearly dependent parameter and, the parameter error is computed for the linearized model. For k =1, the method is monotonic and has a unique solution, for k > 1 non-monotonic.

In the slow method, the output includes the c and the identified, initial condition shape function (Fig A1). Every shape function parameter is non-linearly dependent except the scaling, resulting in large numerical work. The Ci (i=1, 2… 200) values for each shape function are built-in, being determined beforehand.

The initial excess pore water pressure u_0 is the sum of a negative part due to the interface shear in a thin zone along the shaft and a positive part due to the penetration of normal stresses. The first part is described by one of 5 linear functions within the shear zone (between r_0 and r_s). The second part ($r_s < r \le r_1$), is given the function described by (Table A1):

$$u_0(F,r) = \left(1 - e^{\frac{r-r_1}{F}}\right) \Big/ \left(1 - e^{-\frac{r_1-r_s}{F}}\right) \quad F \neq 0; F \neq \infty \tag{1}$$

with fixed F values. Seven r_s values (varying between $0.1r_0$ and $2r_0$) were used, given in Table A1. Hence, 350 shape functions have resulted. For negative scaling, 350 mirror image shape functions have resulted.

Table A1. Thickness values of the interface shear zone

s [-]	t_s [cm]	$r_s = r_o + t_s$ [cm]	$s = t_s/r_o$ [-]
1	0.1	1.85	0.05
2	0.21	1.96	0.12
3	0.42	2.17	0.24
4	0.84	2.59	0.48
5	1.89	3.64	1.08
6	2.94	4.69	1.68
7	3.36	5.11	1.92

1.2. Some notes on the evaluation of simple qc tests

Some empirical parameters have been defined for the characterization of the simple rheological-type cone penetration test records (Imre 1995, Figs 10 to 12), which are supported by the parameters inferred from theoretical data shown in Figure 5 (see Figs 13, 14). One such parameter is the local side friction sounding parameter Δf_{s2} is given by:

$$\Delta f_{s2} = f_s(t_i) - f_s(t_i + t_1); \tag{2}$$

where t_i is the time when the immediate stress drop is ended, and t_1 is a reference time of 150 s. The initial tangent parameter ν is defined by fitting the relaxation equation of the Poynting-Thomson model to the cone resistance data. The equation of the model is:

$$\sigma(t) = \sigma_\infty + (\sigma_0 - \sigma_\infty)\, e^{-\frac{t}{\upsilon}} \tag{3}$$

The verification of these equations is as follows.

Generally, linear consolidation model is used, since unloading takes place around the shaft after penetration.

The consolidation model for the pore water pressure can be two dimensional, uncoupled with a numerical solution that is less favorable from the point of view of inverse problem solution (see e.g. Teh and Houlsby, 1988).

Alternatively, the model can be one dimensional with an analytical solution which is more favorable from the point of view of the inverse problem solution (Table 2, Imre et al., 2010).

The latter form three sets ('families'), the uncoupled, the coupled 1 and the coupled 2 families, consisting of such oedometric, cylindrical and spherical models that have the same set of boundary conditions and assumptions.

The total stress dissipation is the sum of two terms that originated from relaxation and from consolidation being influenced by the initial

mean pore water pressure distribution. All parameters are dependent on the soil type. The time variation of the effective stress (Fig. A-1) is determined by the opposite effect of the coefficient of consolidation (*c*) and the coefficient of relaxation (s) for a fixed initial condition. It is influenced by the initial mean pore water pressure distribution, also. All parameters are dependent on the soil type. It can be shown that this dependence can be used to verify the foregoing empirical parameters.

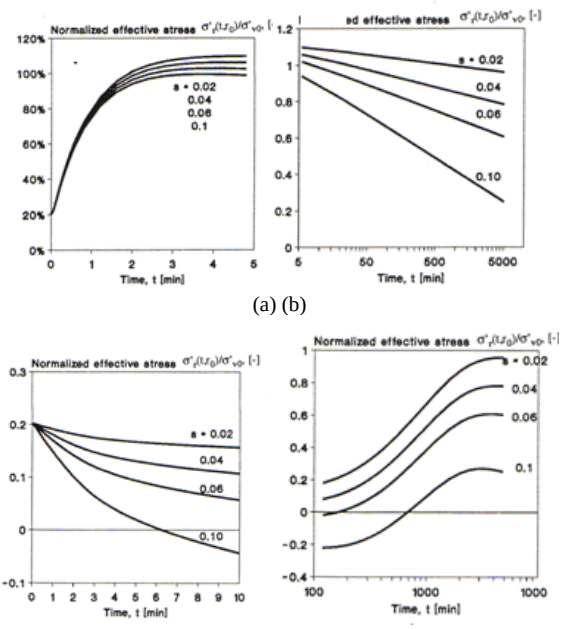

(a) (b)

(c) (d)

Figure A-1. Joined model, effective radial stresses on the shaft, for a fixed initial l condition, in the function of the coefficient of relaxation s. a. short term behaviour, c_v = le-3 m2/s, b. short term behaviour, c_v = le-8 m2/s; c. long term behaviour, c_v = le-8 m2/s. Therefore, the behavior is opposite for sands and clays on a short and long term basis.

1.3. Some notes on the compression test models

The oedometric compression test data can be evaluated as follows. The displacement at the sample top (y=0) for the model AC (i.e. the modified model Bjerrum ([6]):

$$v(t,0) = v_0 + v_1(t,0) + v_2(t,0) \quad (4)$$

where superscripts 0, 1, 2 indicate immediate, consolidation and creep, respectively. The creep term:

$$v_2(t,0) = C_\alpha \frac{2H}{1+e_0} \log\frac{t}{t_1}; t > t_1 \quad (5)$$

where C_α is the coefficient of creep, and t_1 is time parameter, t is time; $2H$ is sample height, e_0 is initial void ratio. The consolidation term is computed with the Terzaghi's model, depending on the maximum compression $v_{1,\max} = 2H\sigma / E_s$ where σ is total stress, E_s is oedometric modulus and the coefficient of consolidation *c*. In model A (i.e. the modified model of Terzaghi) the creep term is missing.